



## Joint Energy Detection and Massive Array Design for Localization and Mapping

Francesco Guidi, Anna Guerra, Davide Dardari, Antonio Clemente, Raffaele d'Errico

### ► To cite this version:

Francesco Guidi, Anna Guerra, Davide Dardari, Antonio Clemente, Raffaele d'Errico. Joint Energy Detection and Massive Array Design for Localization and Mapping. *IEEE Transactions on Wireless Communications*, 2016, 16, pp.1359 - 1371. 10.1109/TWC.2016.2627032 . cea-01559003

HAL Id: cea-01559003

<https://cea.hal.science/cea-01559003>

Submitted on 10 Jul 2017

**HAL** is a multi-disciplinary open access archive for the deposit and dissemination of scientific research documents, whether they are published or not. The documents may come from teaching and research institutions in France or abroad, or from public or private research centers.

L'archive ouverte pluridisciplinaire **HAL**, est destinée au dépôt et à la diffusion de documents scientifiques de niveau recherche, publiés ou non, émanant des établissements d'enseignement et de recherche français ou étrangers, des laboratoires publics ou privés.

# Joint Energy Detection and Massive Arrays Design for Localization and Mapping

Francesco Guidi *Member, IEEE*, Anna Guerra *Member, IEEE*, Davide Dardari *Senior, IEEE*, Antonio Clemente *Member, IEEE*, Raffaele D'Errico *Member, IEEE*

**Abstract**—The adoption of massive arrays for simultaneous localization and mapping (SLAM) or personal radar applications enables the possibility to detect and localize surrounding objects through an accurate beamforming procedure. Unfortunately, when a classical constant false alarm rate (CFAR) approach accounting for ideal-pencil beam pattern is adopted, ambiguities in signal detection could arise due to the presence of side-lobes which can cause non-negligible errors in target detection and ranging. To counteract such effect, in this paper we propose a joint threshold-array design approach where the antenna characteristics are taken into account to best set the threshold and to guarantee the desired detection and ranging performance at the non-coherent receiver section. In order to consider realistic arrays impairments, we focus our attention on the number of antenna elements and of phase shifter bits used for beamforming as key players in defining a trade-off between structural complexity, well-defined radiation pattern and high localization performance. Simulation and measurement results show that the number of bits per phase shifter can be relaxed in favor of a simpler array design, if the number of antennas is sufficiently high and the side-lobes are kept within a suitable level allowing a desired robustness to interference signals.

**Index Terms**—Massive arrays, personal radar, target detection, side-lobes.

## I. INTRODUCTION

Nowadays, several studies are focusing towards the miniaturization and the adoption of large scale arrays [1] for mobile communication [2] or for ranging and localization applications, such as SLAM [3], [4] and personal radar [5], thanks to the possibility to achieve a precise and high-scanning resolution given by the large number of adopted antennas [6]–[9].

SLAM applications, based on the concept that a user or a robot moving in an unknown environment recognizes and localizes the surrounding objects, require both high-definition distance estimates (accurate ranging capabilities) and very narrow steering beams (high angular resolution) [3], [4]. Analogously, the concept of personal radar has been recently proposed in [5], [10] where it has been shown the possibility to jointly exploit millimeter-waves (mmW) and wideband massive arrays technologies for indoor environment mapping

F. Guidi, A. Clemente and R. D'Errico are with CEA, LETI, MINATEC Campus, 38054 Grenoble, France. They are also with Univ. Grenoble Alpes, 38000 Grenoble, France. e-mail:{francesco.guidi, antonio.clemente, raffaele.derrico}@cea.fr

A. Guerra and D. Dardari are with the Dipartimento di Ingegneria dell'Energia Elettrica e dell'Informazione “Guglielmo Marconi” - DEI, University of Bologna, Via Venezia 52, 47521 Cesena, ITALY. (e-mail: {anna.guerra3, davide.dardari}@unibo.it).

using portable devices. Thanks to these technologies and to the possibility to electronically steer the beam, there will be the opportunity to avoid the adoption of a dedicated high-directional antenna with mechanical steering capabilities, as proposed in [3], [4], which can not be easily integrated into portable radar devices. Moreover, the near-pencil beam of massive arrays returns a precise angle and range information thus making possible an accurate modeling and characterization of the environment.

Wideband signals are the best candidate to achieve high ranging performance jointly with massive arrays [11]–[14], but the adoption of precise and costly phase shifters and delay lines becomes necessary to assure an accurate signal alignment. Controlled phase shifters implementing a discrete set of phase shifts represent a cheaper alternative which guarantees to reduce the complexity of the biasing network and steering logic, the insertion loss and the overall cost of the antenna system [15], but at the expense of quantization errors [10], a reduced signal alignment and an increased level of side-lobes [9], [15]–[18]. Some new solutions have been investigated in [19] to find a compromise between the number of elements, their spacing and the phase shifters accuracy.

Despite the high-ranging accuracy which can be achieved by the adoption of such systems, all these arrays design characteristics have to be accounted for when target detection is performed by exploiting measurements coming from different steering directions. In the considered scenario, the ranging process is operated as follows: for each steering direction, a train of pulses is transmitted and the environmental response is collected and associated to the pointing angle. Unfortunately, due to the not ideal beam shape, reflections coming from angles different from the intended one might create interference due to side-lobes. In fact, the side-lobes of realistic radiation patterns might cause false target detection, or errors in the ranging procedure, i.e. the distance of target 1 and 2 of Fig. 1 may be confused [20].

According to the current state of the art, classical techniques concern digital beamforming, coherent receiver architectures or iterative and complex adaptive approaches, whereas here we investigate the use of an energy-based receiver (i.e. non-coherent) for analog beamforming for personal radar applications. In particular, in [21] an adaptive approach is shown so that the phase shifters are updated to have pattern nulls towards desired directions. Apart from the different architecture, the complexity here required to solve the side-lobes issue is much higher, as well as when side-lobes cancellers are implemented, as in [22], [23]. In [24] a generalized likelihood ratio test

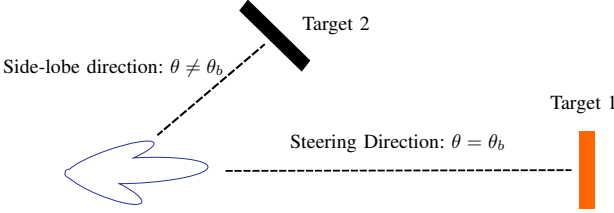


Fig. 1. Considered scenario, where for a steering direction  $\theta_b$ , the signal reflected from an interferer (target 2) in the side-lobe direction is collected together with that coming from the useful target (target 1).

(GLRT) is used to conceive an adaptive decision scheme based on the detection of coherent pulses in presence of Gaussian disturbances. Another possibility consists in the adoption of a side-lobe blanker. In particular, a guard channel, which can be omni-directional and provided by a single array element, is implemented to eliminate impulsive interference (hostile or from other neighboring radars) [25], [26]. All these solutions are usually based on coherent receivers [27] that entail a too high computational complexity for the considered massive arrays especially when operating at mmW frequencies. In addition, in [28], [29], the CLEAN technique to mitigate the image artifacts due to the side-lobes of arrays is reported.

Energy detectors have also been considered jointly with multi-antenna systems: in [30], the receiver architecture is replicated for each antenna and array quantization bits are not accounted for, whereas in [31], only the evaluation of the theoretical performance limits is performed in the presence of the only noise, and thus neglecting all the issues herein analyzed. In [32], a hybrid analog-digital beamforming scheme which is quite insensitive to phase shifters errors is shown. Unfortunately, the phased array structure is divided into several sub-arrays, thus increasing the overall complexity.

In this paper we propose a low-complexity non-coherent detection scheme, where the objects/targets detection and localization is performed by a massive array. In our specific scenario, a unique receiver section is considered where the signals received at each antenna branch are properly combined by phase shifters blocks. Then, the collected measurements become the input of a low-complexity energy detector and the correspondent energy profiles are accumulated over the number of transmitted waveforms. Finally, the last step is a threshold-based detector whose task is to decide if a target is present or not in the steering direction and to determine its position or distance. Thanks to the high number of antennas deployed, it is possible to steer the array beam in different directions in order to detect and localize objects with high accuracy precision. Note that by collecting all the time-of-arrivals (TOAs) and energies of the bins over the threshold for all steering directions it is possible to have a partial map of the surrounding environment. Stimulated by classical signal detection approaches shortcomings, we then take into account the real massive arrays characteristics, e.g. side-lobes, for the threshold evaluation, and we show a set of guidelines to be followed for the array design and choice.

To sum up, accounting for the partially non-coherent receiver based on energy detection previously described, the key

contributions are as follows. We first propose the joint threshold and massive arrays design to improve the localization performance when the aforementioned non-coherent detector is adopted. In addition, according to the considered threshold, it is possible to define a set of array characteristics which let to achieve the desired performance. Successively, through a case study at mmW, we evaluate the performance of the proposed system by means of simulated and measured data, where we exploited a real massive array with 400 elements and only 1-bit of phase quantization. From the obtained results, we show that the joint array-threshold design herein proposed lets to relax the requirements in terms of quantization bits used for single array elements.

The rest of the paper is organized as follows. In Sec. II, the receiver architecture is described. The threshold design with ideal pencil-beams is shown in Sec. III, as well as the impact of real massive arrays on detection performance when such approach is adopted. Sec. IV shows the proper threshold design accounting for antennas non-idealities, and a set of guidelines for the proper array choice. Finally, in Sec. V we report a case study where simulated and real transmitarrays (TAs), adopted as massive arrays, are considered.

## II. RECEIVER ARCHITECTURE

As previously underlined, the localization and mapping applications are based on the idea that the surrounding objects are detected thanks to the beamforming procedure enabled by massive arrays.

The system herein considered exploits a monostatic scattering, i.e., the transmitter and receiver are co-located. For each steering direction  $\theta_b$ ,<sup>1</sup> the massive array steers its beam towards that direction, transmits a train of  $N_p$  pulses and collects the overall backscattered response in order to detect and determine the distance with respect to the pointed object (ranging). This mechanism permits to estimate the range between the radar and the pointed target and to associate it with a particular direction in space, thanks to the steering angle, thus inferring a coarse target position estimate.

To keep the receiver complexity affordable, many works have proposed non-coherent architectures for wideband signalling [33], [34]. Here, as a trade-off between complexity and performance, we consider a partially non-coherent receiver based on energy detection performed after the proper combination of all the received waveforms incident on the array.

To this purpose, a unique receiver section is considered where the signals received at each antenna branch are properly combined by phase shifters blocks. According to Fig. 2, after the combination, the signal is first filtered,<sup>2</sup> successively energy evaluation is performed, and then energy bins are accumulated to improve the signal-to-noise ratio (SNR). Finally, the output of this scheme is compared with a threshold in order to decide whether a target is present or not, and its joint ranging and steering information let to localize it.

<sup>1</sup>For the sake of simplicity, here we consider a 2D scenario. The representation can be extended to the 3D case by accounting for  $\phi_b$ .

<sup>2</sup>By accounting for massive arrays as in [15], [18], signals are directly combined, and it is not possible to process the single element signal.

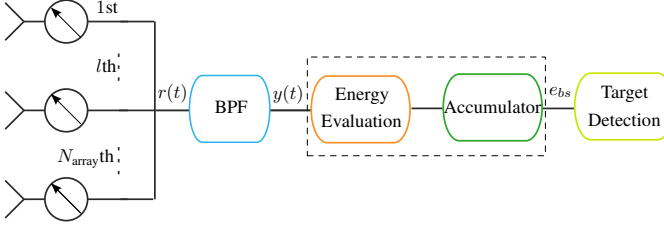


Fig. 2. Considered receiver scheme, where  $N_{\text{array}}$  is the number of antennas in the considered massive array.

In order to describe the signalling scheme, let  $\theta_b = -\theta_b^{\max}/2 \left( \frac{N_{\text{steer}}-1}{N_{\text{steer}}} \right) + (b-1)\theta_b^{\max}/N_{\text{steer}}$ ,  $b = 1, 2, \dots, N_{\text{steer}}$ , be the considered  $N_{\text{steer}}$  steering directions during the scanning process, and  $\theta_b^{\max}$  the maximum scanning range according to the considered arrays configuration.<sup>3</sup>

Consider a generic interrogation signal composed of  $N_p$  pass-band pulses  $p(t)$  of large bandwidth  $W$

$$g(t) = \sum_{l=0}^{N_p-1} p(t-lT_f) \quad (1)$$

with  $T_f$  being the time frame chosen so that all signals backscattered by the environment are received before the transmission of the successive pulse, thus avoiding inter-frame interference. The consequent scanning time is  $T_{\text{scan}} = T_{\text{ob}}N_{\text{steer}}$ , where  $T_{\text{ob}} = N_p T_f$ .

Since each pulse is backscattered by the surrounding targets populating the environment, for the steering direction  $\theta_b$  the received signal can be expressed as

$$r(t, \theta_b) = \sum_{l=0}^{N_p-1} x(t-lT_f, \theta_b) + n(t) \quad (2)$$

where  $x(t, \theta_b)$  is the channel response to the transmitted pulse  $p(t)$  at direction  $\theta_b$ ,<sup>4</sup> and with  $n(t)$  being the additive white gaussian noise (AWGN) with two-sided power spectral density  $N_0/2$ .

The received signal is first passed through an ideal band-pass filter (BPF) with center frequency  $f_c$  to eliminate the out-of-band noise.<sup>5</sup> The filtered signal is denoted by

$$y(t, \theta_b) = \sum_{l=0}^{N_p-1} \tilde{x}(t-lT_f, \theta_b) + z(t) \quad (3)$$

where  $\tilde{x}(t, \theta_b) = x(t, \theta_b) \otimes h_F(t) \cong x(t, \theta_b)$  and  $z(t) = n(t) \otimes h_F(t)$ , with  $h_F(t)$  being the impulse response of the BPF filter reported also in Fig. 2.

To conjugate the need of having a manageable number of measurements and a low complexity receiver, we consider a non-coherent approach based on energy measurements in a discretized time scale which accounts for the complete uncertainty on the received waveform shape. Specifically, energy measurements are taken during the time frame  $T_f$  after the

<sup>3</sup>Ideally,  $\theta_b^{\max} = 90^\circ$ . Unfortunately, due to the array characteristics, it is often limited to around  $60^\circ$ .

<sup>4</sup> $\otimes$  is the convolutional operator.

<sup>5</sup>This operation is necessary since the receiver is energy-based, as it will be described later.

transmission of each pulse by subdividing the time frame into  $N_{\text{bins}} = \lfloor T_f/T_{\text{ED}} \rfloor$  time slots (bins) of duration  $T_{\text{ED}}$ . Note that  $T_{\text{ED}}$  must be chosen to accommodate most of the energy of the received pulse, i.e.  $T_{\text{ED}} \approx 1/W$ . Energy measurements are accumulated for each time bin over the  $N_p$  frames of the interrogation signal. The accumulated energy measurement at the  $s$ th time bin and  $b$ th steering angle, corresponding to the respective blocks of Fig. 2, is

$$e_{bs} = \sum_{k=0}^{N_p-1} \int_{(s-1)T_{\text{ED}}}^{sT_{\text{ED}}} y^2(t+kT_f, \theta_b) dt \quad (4)$$

with  $s = 1, 2, \dots, N_{\text{bin}}$  and  $b = 1, 2, \dots, N_{\text{steer}}$ .

According to [35], [36], for each energy bin, the normalized energy measurement output can be well approximated by

$$\Lambda_{bs} = \frac{2}{N_0} e_{bs} \simeq \frac{1}{\sigma^2} \sum_{k=0}^{N_p-1} \sum_{i=(s-1)N_d}^{sN_d} \left( x_i(\theta_b) + z_i^{(k)} \right)^2 \quad (5)$$

where  $N_d = 2WT_{\text{ED}}$ ,  $\sigma^2 = N_0W$  is the noise variance, and  $z_i^{(k)}$  are for odd  $i$  (even  $i$ ) the samples of the real (imaginary) part of the equivalent low-pass of  $z(t+kT_f)$ ,  $k = 1, 2, \dots, N_p$ , taken at Nyquist rate  $W$  in each interval  $T_{\text{ED}}$ . In (14) we used the property  $x(t+kT_f, \theta_b) = x(t, \theta_b)$ , with  $k = 1, 2, \dots, N_p$ , so that  $x_i(\theta_b)$  represents for odd  $i$  (even  $i$ ) the samples of the real (imaginary) part of the equivalent low-pass of  $x(t, \theta_b)$ , taken at Nyquist rate  $W$  in each interval  $T_{\text{ED}}$ , which does not depend on  $k$ .

Define now, for each energy bin, the normalized energy detector test

$$\Lambda_{bs} = \frac{2}{N_0} e_{bs} \stackrel{\mathcal{D}_1}{\gtrless} \stackrel{\mathcal{D}_0}{\lessdot} \xi_{bs} \quad (6)$$

where  $\xi_{bs}$  being the threshold for the  $b$ th steering direction and  $s$ th bin. The presented decision rule consists in

$$\text{Decide : } \begin{cases} \mathcal{D}_0, & \text{if } \Lambda_{bs} < \xi_{bs} \quad \forall \{s\}, \\ \mathcal{D}_1, & \text{if } \exists \{s\} \text{ s.t. } \Lambda_{bs} \geq \xi_{bs} \end{cases} \quad (7)$$

where  $\mathcal{D}_1$  and  $\mathcal{D}_0$  represent the state in which at least a target overcomes or not the threshold in direction  $\theta_b$ , respectively. If the threshold is exceeded for the first time at  $s = \hat{s}$ , the coordinate  $\hat{s}$  leads to an estimate of the target TOA ( $\hat{\tau} = \hat{s} \cdot T_{\text{ED}} - T_{\text{ED}}/2 \approx \hat{s} \cdot T_{\text{ED}}$ ) and, jointly with the steering direction  $\theta_b$ , it provides the spatial position of the target in the surrounding environment.

In the next section, we evaluate the impact of real arrays side-lobes on the detection performance when ideal pencil beam antennas are accounted for in the threshold design.

### III. EFFECT OF REALISTIC MASSIVE ARRAYS ON DETECTION PERFORMANCE

#### A. Detection Threshold with Ideal Pencil Beam Patterns

As previously underlined, when an ideal pencil-beam antenna is considered, we aim to preserve that the probability of a false alarm event due to the receiver noise does not exceed

a certain value. Thus, in the presence of only the noise, i.e.  $y(t, \theta_b) = z(t)$ , eq. (5) can be written as

$$\Lambda_{bs} \simeq \frac{1}{\sigma^2} \sum_{k=0}^{N_p-1} \sum_{i=(s-1)N_d}^{sN_d} \left( z_i^{(k)} \right)^2. \quad (8)$$

In (8) we have the sum of the square of  $N = N_p N_d$  independent Gaussian random variables (RVs) which turns out into a central Chi-square distribution, with  $N$  degrees of freedom [37] with probability density function (PDF)

$$f_C(y, \nu) = \frac{y^{(\frac{\nu}{2}-1)}}{2^{\frac{\nu}{2}} \Gamma(\frac{\nu}{2})} e^{-\frac{y}{2}} \quad y \geq 0, \quad (9)$$

having denoted with  $\Gamma(\cdot)$  the gamma function [37, p. 255]. Now consider to apply the threshold for each steering direction. A threshold-crossing event at the  $s$ th bin, that is  $\{\Lambda_{bs} \geq \xi_{bs}\}$ , results in a single-bin probability of false alarm (PFA)  $p_{bs}^{(FA)}$  given by [38]

$$p_{bs}^{(FA)} = \int_{\xi_{bs}}^{\infty} f_C(y, N) dy = \frac{\Gamma(\frac{N}{2}, \frac{\xi_{bs}}{2})}{\Gamma(\frac{N}{2})} = \tilde{\Gamma}\left(\frac{N}{2}, \frac{\xi_{bs}}{2}\right) \quad (10)$$

where  $\Gamma(a, x) = \int_x^{\infty} x^{a-1} e^{-x} dx$  is the upper incomplete gamma function and  $\tilde{\Gamma}(\cdot, \cdot)$  is the gamma regularized function. The threshold can be computed starting from a requirement on the global PFA  $P_{FA}^*$  accounting for all bins at the  $b$ th steering direction. Note that in the presence of the only noise, the single-bin false alarm probability results to be the same in each bin, that is  $p_{bs}^{(FA)} = p_{FA}$ ,  $\forall \{b, s\}$ , which means

$$P_{FA}^* = 1 - \prod_{s=1}^{N_{bins}} \left( 1 - p_{bs}^{(FA)} \right) \approx N_{bins} \cdot p_{FA} \quad (11)$$

where we have assumed that all bins are statistically independent and  $p_{bs}^{(FA)} \ll 1$ . Equation (11) translates into a required  $P_{FA}^*$  per bin given by

$$p_{FA}^* \approx \frac{P_{FA}^*}{N_{bins}}. \quad (12)$$

Finally we can write

$$\xi = 2 \left[ \text{Inv} \tilde{\Gamma} \left( \frac{N}{2}, \frac{P_{FA}^*}{N_{bins}} \right) \right] \quad (13)$$

where  $\text{Inv} \tilde{\Gamma}(\cdot, \cdot)$  is the inverse gamma regularized function (if  $w = \tilde{\Gamma}(a, z)$ , then  $z = \tilde{\Gamma}^{-1}(a, w)$ ). Note that with such approach, the threshold does not depend on the bin and steering indeces, i.e.  $\xi_{bs} = \xi$  and it is set to keep the PFA due to the receiver noise to a desired value  $P_{FA}^*$ . In the following, we first introduce the arrays characteristics, and then we analyse the effects of real arrays when the target detection approach previously described is adopted.

### B. Detection Performance with Realistic Arrays

1) *Antenna Array Characteristics:* The analysis herein presented can be applied to any frequency band although constraints in terms of the number of antennas might be relevant depending on the antenna technology and the intended angular resolution. At microwave frequencies the antenna

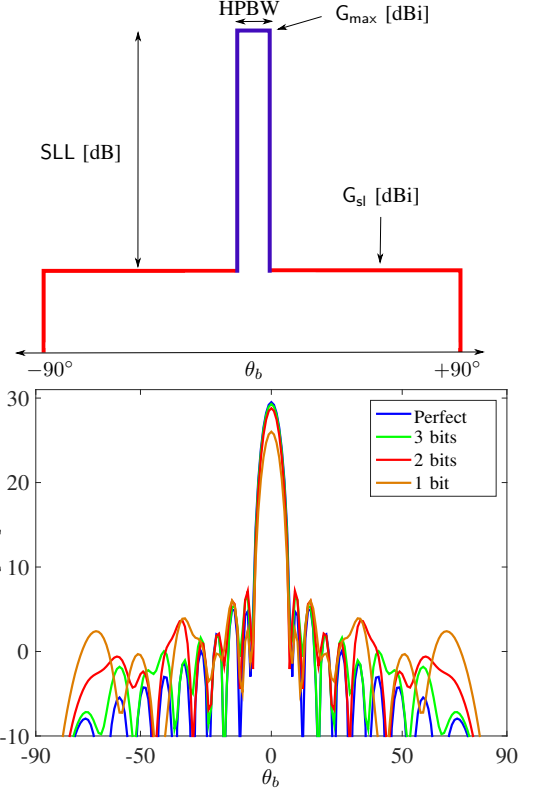


Fig. 3. Mask definition for massive array design (top) and example of  $20 \times 20$  arrays gains (bottom) for different phase quantization.

array technology is quite mature but device dimensions limit the maximum integrable number of antenna elements, whereas at mmW severe technological constraints are still present and must be taken into account even though significant progresses have been recently done [39].

As previously pointed out, a large bandwidth is in general desirable thanks to the corresponding achievable high ranging resolution. However, in a wideband system, the received signal arrives at each antenna element with a delay that is not negligible compared to the signal duration, and hence it cannot be compensated by adopting only phase shifters, as typically done in narrowband systems. Unfortunately, the adoption of a huge number of time delay circuits could represent a high-cost and, at the moment, impractical solution especially at mmW frequencies. Consequently, phase shifters remain the most viable solution [40]. Thus, in the absence of time delays, the accumulation of the component received by each branch may result in a signal shape distortion.

One of the most interesting antenna geometric configuration is the planar array, which can be exploited in several applications thanks to its simple and compact architecture. In practical cases, the directivity might be affected by several factors [41]. As an example, ideally it is expected to have a continuous phase in phase shifters, in order to maximize the signal re-combination and thus the gain. Instead, when 1-bit of phase quantization is adopted, it implies that there are only two possible phases for signals for their re-combination:  $0^\circ$  or  $180^\circ$ . Analogously, for  $n$ -bits there are  $2^n$  possible available phases. In [18] it is shown that the adoption of only 1 bit

causes a directivity loss of few dBi. In addition, the gain could be some few dBs lower due to insertion and, in case of an external source, spillover losses.<sup>6</sup> Three main effects can be experienced due to phase quantization: (i) Reduction of array aperture efficiency; (ii) Impact on the SLL; (iii) Impact on the steering performance. While the first two effects are more dominant, the steering error is quite marginal and can be neglected, as reported in [9]. Thus, despite the high gain which can be guaranteed by multi-antenna systems, the idea to consider massive arrays as laser-beam antennas is only an approximation and the presence of side-lobes could compromise target detection and localization.

According to Fig. 3, consider the following massive array parameters which are accounted for in our work:

- half power beamwidth (HPBW): it represents the half-power beamwidth required to guarantee good angular resolution and scanning performance;
- $G_{\max}$ : it represents the required maximum gain to achieve the desired target detection performance in the intended direction;
- $G_{\text{sl}}$ : the maximum gain in the side-lobe direction;
- SLL: from the previous two parameters, it is possible to set the side lobe level (SLL) as  $\text{SLL} [\text{dB}] = G_{\text{sl}} [\text{dBi}] - G_{\max} [\text{dBi}]$ . In addition, we define  $\Omega = 1/\text{SLL}$ .

Such mask has to be evaluated in order to guarantee angle resolution and good detection performance as well as robustness against the interference signals.

2) *Evaluation of the side-lobes impact*: The threshold of Sec. III-A has been derived accounting for the presence of the noise receiver only and ideal laser-like radiation pattern.

This approximation might be coarse when the previously described real arrays are adopted, as shown in Fig. 1, due to the backscattered signal components coming from different directions not filtered by the antenna pattern because of sidelobes. Thus, we evaluate the impact of side-lobes when such approach is adopted. Define  $x_{\text{sl}}(t, \theta_b)$  the received backscattering response under the assumption that no target is in the steering direction  $\theta_b$ , i.e. the target 1 of Fig. 1 is not present. Due to the presence of signals coming from side-lobes direction, the normalized decision variable results in

$$\Lambda_{bs} = \frac{2}{N_0} e_{bs} \simeq \frac{1}{\sigma^2} \sum_{k=0}^{N_p-1} \sum_{i=(s-1)N_d}^{sN_d} \left( x_{\text{sl}_i}(\theta_b) + z_i^{(k)} \right)^2 \quad (14)$$

where  $x_{\text{sl}_i}(\theta_b)$  are the sampling expansion coefficients of  $x_{\text{sl}}(t, \theta_b)$ . In (14) we have that the energy output corresponding to the generic bin is now distributed as a non-central Chi-square distribution. In particular, the presence of  $x_{\text{sl}_i}(\theta_b)$  leads to the non-centrality parameter (NCP)  $\lambda_{bs} = 2\gamma_{bs}$  [35], [42], where  $\gamma_{bs}$  is the side-lobe-to-noise ratio (SLNR) per bin, given

<sup>6</sup>Spillover losses are present when the multi-antenna structure is excited by an external source spatial feed as in the case of reflect- and transmitarrays, and a part of the power emitted by the focal source is not intercepted by the array aperture. Analogously, if the focal source is too close, the array surface could be badly illuminated resulting in a low taper efficiency. Practically, a trade-off is necessary between the spill-over loss, taper efficiency, and bandwidth.

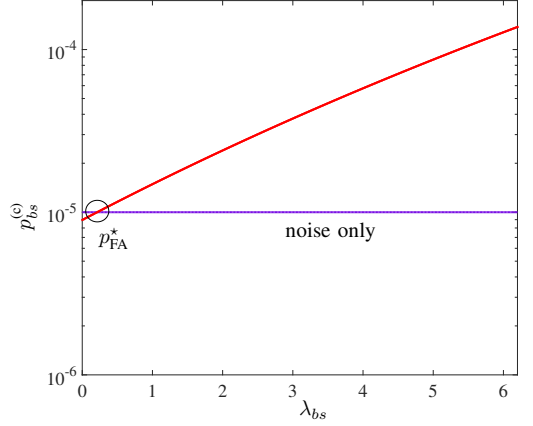


Fig. 4. Bin-crossing probability when the threshold  $\xi$  of (13) is adopted and  $p_{\text{FA}}^* = 10^{-5}$ .

by

$$\gamma_{bs} \simeq \frac{1}{2\sigma^2} \sum_{i=0}^{N_p-1} \sum_{i=(m-1)N}^{mN} (x_{\text{sl}_i}(\theta_b))^2 \quad (15)$$

with  $N = N_p N_d$  degrees of freedom. Note that (15) represents the accumulated SLNR corresponding to the  $s$ th time bin and the  $b$ th steering direction which increases with the number  $N_p$  of pulses which serves to improve the SNR at the expense of an increased scanning time.

A threshold-crossing event at the  $s$ th bin results in a single-bin side-lobes crossing probability (SCP)  $p_{bs}^{(c)}$  given by [38]

$$p_{bs}^{(c)} = Q_h \left( \sqrt{\lambda_{bs}}, \sqrt{\xi_{bs}} \right) \quad (16)$$

with  $Q_h(\alpha, \beta) = \int_{\beta}^{\infty} x (\frac{x}{\alpha})^{h-1} \exp\left(-\frac{x^2 + \alpha^2}{2}\right) I_{h-1}(\alpha x) dx$  denoting the generalized Marcum's  $Q$  function of order  $h = N/2$  [43]. Ideally, it is desired to have  $p_{bs}^{(c)} = p_{\text{FA}}^*$  since the signals component deriving from side-lobes direction is unwanted.

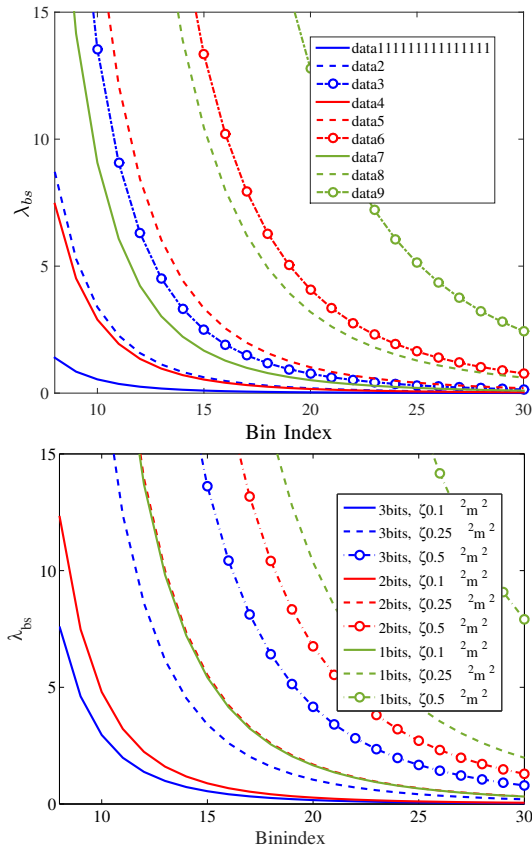
Then, we numerically evaluate the effects of constant threshold design in (13) considering the presence of side-lobes. In particular, unless otherwise indicated, we consider a time frame  $T_f = 100$  ns,  $W = 1$  GHz,  $T_{\text{ED}} = 1$  ns, a receiver noise figure of  $N_F = 4$  dB with  $T_0 = 290$  K, and an effective radiated isotropic power (EIRP) of 30 dBm, compliant with the Federal Communications Commission (FCC) regulations. In this way, by setting an overall  $P_{\text{FA}}^* = 10^{-3}$ , it is  $p_{\text{FA}}^* = 10^{-5}$  which gives the threshold  $\xi$  according to (13). By considering (16), it is possible to estimate such effects when  $\lambda_{bs}$  is greater than 0. The obtained results are reported in Fig. 4, where it is evidenced that only for  $\lambda_{bs} < 0.5$ , the single bin  $p_{bs}^{(c)}$  is still close to the desired value of  $10^{-5}$ . Consequently, the system is not robust for target detection, as it is extremely sensitive to the presence of a target outside  $\theta_b$ .

In order to find possible practical values of  $\lambda_{bs}$ , a simple solution is to consider free-space propagation from the target to the TX/RX section, and to assume the entire backscattered energy contained into one bin, which represents a worst case scenario. Successively, we dimension  $\lambda_{bs}$  as a function of the expected path-loss of the signal in each bin from a side-lobe

TABLE I

SIDE-LOBES LEVEL AND MAXIMUM GAIN OF  $15 \times 15$  TA AT  $f_c = 60$  GHz.

$\theta_b = 0^\circ$			
Quantization	$G_{\max}$ [dBi]	SLL [dB]	HPBW ( $^\circ$ )
No quantization	27.1	-23.3	$\approx 8$
3 bits	26.9	-24.6	$\approx 8$
2 bits	26.4	-20.6	$\approx 8$
1 bit	23.5	-16.8	$\approx 8$
$\theta_b = 20^\circ$			
Quantization	$G_{\max}$ [dBi]	SLL [dB]	HPBW ( $^\circ$ )
No quantization	26.8	-22.8	$\approx 9$
3 bits	26.5	-20.7	$\approx 9$
2 bits	25.9	-19.4	$\approx 9$
1 bit	22.2	-13.6	$\approx 9$

Fig. 5. NCP values for different values of  $\zeta$  and for  $\theta_b = 0^\circ$  (top) and  $\theta_b = 20^\circ$  (bottom).

direction. We obtain

$$\lambda_{bs} = 2\gamma_{bs} = \frac{1}{\sigma^2} \int_W S(f) \cdot G_{\text{sl}}^2(f) \zeta \frac{c^2}{f^2 (4\pi)^3 d_s^4} df \quad (17)$$

where  $\zeta$  is the target radar cross-section in the side-lobe direction,<sup>7</sup>  $G_{\text{sl}}(f)$  is the maximum side-lobe gain,  $S(f)$  is the transmitted power spectral density (PSD) set according to the EIRP, and  $d_s$  is the target-array distance, concerning the  $s$ th bin.

<sup>7</sup>Note that here we neglected the dependency of  $\zeta$  with the frequency.

As real massive arrays, we consider  $15 \times 15$  TAs which are possible candidates for this kind of applications due to their narrow beam [10], as described also in the next section, by accounting for a different number of quantization bits which impact in the array pattern.

The considered TA is composed of a focal source illuminating a planar array whose building blocks are called unit-cells, spaced apart of  $\lambda_0/2$ , where  $\lambda_0$  is the wavelength at  $f_0 = 60$  GHz. The linearly polarized unit-cell is modelled as a uniform aperture as described in [18]. Since a continuous phase shift between  $0^\circ$  and  $360^\circ$  is ideally required to exactly compensate the phase on the array aperture, a phase quantization was introduced, where a trade-off between complexity and losses has to be accounted for. As an example, Table I reports different values of  $G_{\max}$  and  $G_{\text{sl}}$  evaluated at the central frequency  $f_c = 60$  GHz.<sup>8</sup>

In Fig. 5,  $\lambda_{bs}$  values are reported according to different quantization bits, the bin index (i.e. the target distance from the TX/RX) and different values of  $\zeta$ . From these results, we found that  $\lambda_{bs}$  is often above 0.5, which was previously determined as a limit value in order to preserve  $p_c = p_{\text{FA}}^*$  in the presence of side-lobes. By comparing Fig. 5-(top) and Fig. 5-(bottom), it can be noted that the values of  $\lambda_{bs}$  are also strictly related to the steering direction as the side-lobes level might increase, as also reported in Table I. Indeed, the values of  $\lambda_{bs}$  also change when a low number of quantization bits is adopted. This effect suggests that the side-lobe level should be treated differently for each steering direction and the threshold should account for the low number of phase quantization bits.

In the following we show a possible joint threshold and array design in order to properly set the massive array mask to achieve the desired localization performance.

#### IV. JOINT THRESHOLD AND MASSIVE ARRAY DESIGN

In the previous section, the threshold has been set considering the presence of the noise receiver only and we have shown the strong impact of side-lobes. We now introduce a model for threshold setting which accounts for the possible presence of interference components coming from side-lobes.

##### A. Enhanced Detection Threshold Approach

The adopted model makes use of two approximations. First, we consider the energy deriving from a target entirely included in one energy-bin, as previously done. Second, indicating with  $\hat{s}$  the bin relating to the target in the steering direction, we assume that such bin is always present in the integration window, since we consider indoor environments.

In case the threshold is exceeded in more than one bin for a given steering direction, the simplest strategy is to associate the target position to the earliest element, whose coordinate  $\hat{s}$  provides a coarse TOA estimate. This approach can affect the ranging error, as in our scenario we can foresee the situations depicted in Fig. 6. In particular, when energy-bins due to side-lobes are not detected, we have two cases: no bin crosses

<sup>8</sup>The  $\mathcal{F}/\mathcal{D}$  ratio, with  $\mathcal{F}$  being the focal distance and  $\mathcal{D}$  the array length, has been optimized for maximizing the TA gain [18].

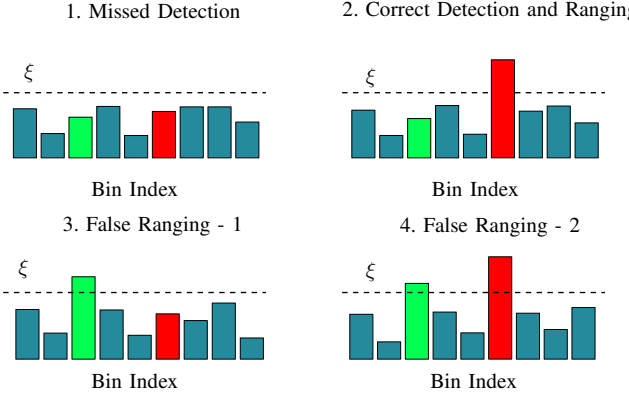


Fig. 6. Situations depicted in our scenario. Red and green colors denote the target and the side-lobe signal, respectively.

the threshold, with a consequent error in the ranging (case 1 of Fig. 6), and the useful  $\hat{s}$  one exceeds the threshold, with the possibility to correctly perform target ranging (cases 2 of Fig. 6). On the contrary, when a side-lobe energy bin  $s$  exceeds the threshold, we can still have a correct-ranging, if  $s > \hat{s}$ , or a false ranging, if  $s < \hat{s}$  (case 4 of Fig. 6) or if the  $\hat{s}$ th bin does not cross the threshold (cases 3 of Fig. 6).

In order to describe the situations previously depicted, we now consider three figures of merit:

- the SCP, i.e. the probability that at least one interference signal exceeds the threshold;
- the probability of false ranging (PFR), i.e. the probability of wrongly deciding that a target is present at a certain distance for a given steering direction due to side-lobes. According to Fig. 6, it relates to the situations 3 and 4, where it is expected that (i) the interference bin index is lower than the useful one overcoming the threshold; (ii) the useful bin does not overcome the threshold, and the interference one can assume any value;
- the probability of correct ranging (PCR), i.e. the probability of taking the correct decision of the target distance from the massive array (case 2 of Fig. 6).

According to the previous results, if the threshold is designed according to the receiver noise only (i.e. accounting for a laser-beam like antenna), the system is not robust to the presence of side-lobes. Therefore, in the following we show a threshold design which accounts for all these effects.

In order to set the threshold, we now consider only signals deriving from the main side-lobe, as they will determine the threshold level, thus neglecting the presence of targets in the steering direction.

Then, the SCP  $P_{\text{SC}}(\theta_b) = P_{\text{SC}}$  for each steering direction is given by

$$P_{\text{SC}} = \left[ 1 - \prod_{s=1}^{N_{\text{bins}}} \left( 1 - p_{bs}^{(c)} \right) \right] \approx N_{\text{bins}} p^{(c)}. \quad (18)$$

where it has been assumed  $p_{bs}^{(c)} = p^{(c)} \forall b$  and  $\forall s$  due to the CFAR approach adopted. The threshold  $\xi_{bs}$ , corresponding to a target overall SCP  $P_{\text{SC}}^*$  can be determined from (16) and

(18) as given by

$$\xi_{bs} = \left[ Q_h^{-1} \left( \sqrt{\lambda_{bs}}, \frac{P_{\text{SC}}^*}{N_{\text{bins}}} \right) \right]^2 \quad (19)$$

where  $P_{\text{SC}}^*$  indicates the desired *a-priori* SCP.

Note that for large  $N$  (typically  $> 50$ ), i.e. for large  $N_p$ , the non-central Chi-square distribution can be approximated with a Gaussian distribution having mean  $\lambda_{bs} + N$  and variance  $2(N + 2\lambda_{bs})$  [44]. Thus, for a given steering direction, we can write

$$p^{(c)} = \frac{P_{\text{SC}}^*}{N_{\text{bins}}} \approx \frac{1}{2} \operatorname{erfc} \left( \frac{\xi_{bs} - (\lambda_{bs} + N)}{2\sqrt{(N + 2\lambda_{bs})}} \right) \quad (20)$$

where  $\operatorname{erfc}(\cdot)$  is the complementary error function.<sup>9</sup> Thus, the threshold per bin can be approximated as follows

$$\xi_{bs} \approx 2\sqrt{(N + 2\lambda_{bs})} \cdot \operatorname{erfc}^{-1} \left( 2 \frac{P_{\text{SC}}^*}{N_{\text{bins}}} \right) + \lambda_{bs} + N. \quad (21)$$

Once the threshold has been set according to  $p^{(c)}$  and the overall SCP, it is possible to determine the SLL required to guarantee the desired performance in terms of correct detection and ranging. To this purpose, we now explicit the PCR for a given steering direction. In particular, we perform correct ranging if

$$\begin{cases} \Lambda_{b\hat{s}} > \xi_{b\hat{s}} & \text{if } s = \hat{s}; \\ \Lambda_{bs} < \xi_{bs} & \forall s < \hat{s}; \end{cases} \quad (22)$$

which gives

$$P_{\text{CR}} = p_{b\hat{s}}^{(c)} \prod_{s=1}^{\hat{s}-1} \left( 1 - p_{bs}^{(c)} \right) \approx p_{b\hat{s}}^{(c)} \left[ 1 - (\hat{s} - 1)p^{(c)} \right] \quad (23)$$

i.e. no crossing event happens before the  $\hat{s}$ th bin. In particular, from (23), it is possible to set the minimum level of maximum gain required in order to have a desired  $P_{\text{CR}}^*$  through the NCP  $\lambda_{b\hat{s}}^{(u)}$ . In fact, we can write

$$p_{b\hat{s}}^{(c)} = Q_h \left( \sqrt{\lambda_{b\hat{s}}^{(u)}}, \sqrt{\xi_{b\hat{s}}} \right) \quad (24)$$

which gives

$$\lambda_{b\hat{s}}^{(u)} = \left[ Q_h^{-1} \left( \frac{P_{\text{CR}}^*}{1 - (\hat{s} - 1) \frac{P_{\text{SC}}^*}{N_{\text{bins}}}}, \sqrt{\xi_{b\hat{s}}} \right) \right]^2. \quad (25)$$

In our scenario,  $\lambda_{b\hat{s}}^{(u)}$  and  $\lambda_{b\hat{s}}^{(i)}$  refer to the NCP due to the useful and the interference target, respectively. For each bin, we aim to preserve a high detection for  $\lambda_{b\hat{s}}^{(u)}$  whereas  $\lambda_{b\hat{s}}^{(i)}$  has to be masked. Since we aim to explicit the relation between the antenna complexity contained in the SLL with the system performance, we exploit the following relation for the  $\hat{s}$ th bin

$$\begin{aligned} \lambda_{b\hat{s}}^{(u)} &= C_{\hat{s}} \cdot G_{\max}^2 \cdot \zeta_u \\ \lambda_{b\hat{s}}^{(i)} &= C_{\hat{s}} \cdot G_{\text{sl}}^2 \cdot \zeta_i \end{aligned} \quad (26)$$

where  $C_{\hat{s}}$  depends on the propagation losses and on the transmitted power and is fixed for each bin. Thus it is possible

<sup>9</sup>The approximation of (21) is usually valid for high values of  $N$ . In the numerical results case, it will be shown that with accurate values of the NCP, the threshold performs well for the considered scenario.

to write  $G_{\max}/G_{\text{sl}} = \Omega(N_{\text{bit}}) = \sqrt{(\lambda_{b\hat{s}}^{(u)} \zeta_i)/(\lambda_{b\hat{s}}^{(i)} \zeta_u)}$ , which gives

$$\begin{aligned} \Omega(N_{\text{bit}}) &= \frac{1}{\text{SLL}(N_{\text{bit}})} \\ &= \left[ Q_h^{-1} \left( \frac{P_{\text{CR}}^*}{1 - (\hat{s} - 1) \frac{P_{\text{SC}}^*}{N_{\text{bins}}}}, \sqrt{\xi_{b\hat{s}}} \right) \right] \sqrt{\frac{1}{\lambda_{b\hat{s}}^{(i)}} \cdot \frac{\zeta_i}{\zeta_u}}. \quad (27) \end{aligned}$$

Thus, once the  $G_{\text{sl}}$  has been fixed to a certain value, it is possible to find the correspondent  $G_{\max}$  which lets to achieve the desired performance. Consequently, it becomes important to fix the maximum allowable SLL which is strictly related to the array complexity. In fact, the higher  $N_{\text{bit}}$ , the better is the difference between the main peak and the side-lobe. In summary, (27) expresses the trade-off between array complexity and performance which should be carefully accounted for in the system design phase.

Finally, according to Fig. 6, the PFR  $P_{\text{FR}}$ , that is the probability that the target is correctly detected, but the wrong bin is estimated for the TOA, is given by

$$\begin{aligned} P_{\text{FR}} = & p_{b\hat{s}}^{(c)} \left[ 1 - \prod_{s=1}^{\hat{s}-1} \left( 1 - p_{bs}^{(c)} \right) \right] \\ & + \left( 1 - p_{b\hat{s}}^{(c)} \right) \left[ 1 - \prod_{\substack{s=1 \\ s \neq \hat{s}}}^{N_{\text{bins}}} \left( 1 - p_{bs}^{(c)} \right) \right]. \quad (28) \end{aligned}$$

The first addendum in the right-hand side of (28) is related to the case in which, despite the bin in the steering direction overcomes the threshold, a bin due to side-lobes creates ambiguity as it arrives before the useful one (see Fig. 6-bottom right). On the other side, the second addendum of (28) related to Fig. 6 bottom-left, concerns the case when a missed detection of the useful bin takes place, and the bin due to side-lobes overcomes the threshold without the constraint that it should be before the useful one.

According to the derived metrics, in the following we propose a set of guidelines for choosing the best array configuration in order to achieve the desired performance.

### B. Mask Definition and Arrays Choice

Many parameters can affect the arrays characteristics for the correct antenna choice. Thus, we operate as follows.

- Step 1: We fix the HPBW requirement for beamforming accuracy. In particular, since the scenario where we operate is indoor, a good compromise between scanning resolution and antenna complexity is to set  $\text{HPBW} < 15^\circ$  for all the steering directions, which lets to keep a good trade-off between array complexity and performance [10].
- Step 2: From Table I and II, we found that the configurations which satisfy the aforementioned inequality are  $N_{\text{array}} = 15 \times 15$  and  $N_{\text{array}} = 20 \times 20$ . In fact, for  $\theta_b = 60^\circ$  and  $N_{\text{array}} = 100$ , the HPBW is  $\approx 23^\circ$ , which is greater than  $15^\circ$  even for a perfect phase quantization. In particular, for  $N_{\text{array}} = 20 \times 20$  and  $N_{\text{array}} = 15 \times 15$ , the impact of the number of quantization bits is limited within a variation of  $1^\circ$ . From these chosen arrays, we find a

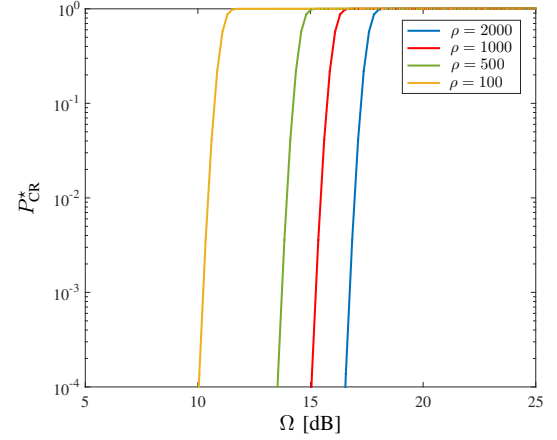


Fig. 7.  $\Omega$  according to different values of  $\rho = \zeta_i/\zeta_u$ .

reasonable  $G_{\text{sl}} = 6$  [dBi]; as shown later, the performance is scaled, and does not depend on the initial  $G_{\text{sl}}$  chosen.

- Step 3: With the initial value of chosen  $G_{\text{sl}}$ , we set the threshold  $\xi_{bs}$ ;
- Step 4: We evaluate the required SLL to achieve the desired performance in terms of correct ranging.

In Fig. 7 we report the different  $\Omega = 1/\text{SLL}$  required to obtain the desired  $P_{\text{CR}}^*$  for some values of  $\rho = \zeta_i/\zeta_u$ , with an initial  $G_{\text{sl}}$  set to 6 dBi for the threshold and by adopting the same parameters as in Sec. III-B2. Note that the value  $\rho = 100$  is roughly estimated from the measurements results described in the following. If we account for  $\rho = 100$  and  $\rho = 500$ , the  $N_{\text{array}} = 20 \times 20$  and  $N_{\text{array}} = 15 \times 15$  configurations guarantee the desired value of around 15–16 dB. Due to the dependency on the SLL, these values do not depend on the initial  $G_{\text{sl}}$  chosen to set the threshold.

According to the mask design and to the Table II, we are now able to choose the massive arrays adequate to accomplish our task, and to evaluate their performance through Monte-Carlo simulations and measured data, as shown in the following.

In the following, starting from the approach herein proposed, we show through a case study the joint array-threshold design which lets also to relax the requirement in terms of quantization bits necessary for the array signals combination.

## V. NUMERICAL RESULTS

In order to evaluate the performance of the described target detection scheme, we now present an example of system design by considering the scheme of Fig. 2.

We consider, as transmitted signal, root-raised cosine pulses compliant with the FCC power emission at 60 GHz, with pulse width parameter  $T_w = 1.6$  ns, roll-off factor  $\beta = 0.6$ , center frequency  $f_c = 60$  GHz. If otherwise indicated, the other parameters are the same as the ones in Sec. III-B2 and Sec. IV-B.

### A. Simulation Results

- 1) *Results with 1 Interferer:* We first investigate the system performance in the presence of only one interferer in the side-lobe direction. In particular, we analyze the overall correct

TABLE II  
SIDE-LOBES LEVEL AND MAXIMUM GAIN AT  $f_c = 60$  GHz FOR  
DIFFERENT PHASE COMPENSATION CONDITIONS, NUMBER OF ANTENNAS  
AND STEERING DIRECTIONS.

$N_{\text{array}} = 10 \times 10, \theta_b = 60^\circ$			
Quantization	$G_{\max}$ [dBi]	SLL [dB]	HPBW ( $^\circ$ )
<b>No quantization</b>	20.1	-9.3	$\approx 24$
3 bits	19.8	-9.2	$\approx 24$
2 bits	18.9	-9.3	$\approx 24$
1 bit	14.3	-3.7	$\approx 26$
$N_{\text{array}} = 20 \times 20, \theta_b = 0^\circ$			
Quantization	$G_{\max}$ [dBi]	SLL [dB]	HPBW ( $^\circ$ )
<b>No quantization</b>	29.5	-24.5	$\approx 6$
3 bits	29.3	-22.8	$\approx 6$
2 bits	28.8	-21.6	$\approx 6$
1 bit	26.0	-18.2	$\approx 6$
$N_{\text{array}} = 20 \times 20, \theta_b = 20^\circ$			
Quantization	$G_{\max}$ [dBi]	SLL [dB]	HPBW ( $^\circ$ )
<b>No quantization</b>	29.3	-27.6	$\approx 6$
3 bits	29.1	-26.9	$\approx 6$
2 bits	28.4	-22.4	$\approx 6$
1 bit	25.2	-17.5	$\approx 6$
$N_{\text{array}} = 20 \times 20, \theta_b = 60^\circ$			
Quantization	$G_{\max}$ [dBi]	SLL [dB]	HPBW ( $^\circ$ )
<b>No quantization</b>	29.5	-26.6	$\approx 11$
3 bits	26.3	-23.1	$\approx 11$
2 bits	25.6	-21.8	$\approx 11$
1 bit	22.3	-14.4	$\approx 11$

detection rate (CDR) as a function of the overall false ranging rate (FRR) in order to estimate the rate of the correct procedure when the target is detected.<sup>10</sup>

If otherwise indicated, for each Monte-Carlo cycle, the useful target has a position which is uniformly distributed between 2 and 10 meters from the radar, whereas the interferer between 2 and 6 meters. For the signal coming from the scatterer, we consider a radar cross section (RCS)  $\zeta_i$  uniformly distributed between 0 and  $\zeta_i^{\max} = 1 \text{ m}^2$  for each cycle. The value of  $1 \text{ m}^2$  has been estimated from the measurement of a metallic plate with size  $0.7 \times 0.7 \text{ m}^2$ , as described in the following paragraph. In particular, we set the desired rates to  $\text{CDR}^* \approx 80\%$  and  $\text{FRR}^* \approx 1\%$  in order to preserve good detection and ranging performance. Since the useful signal energy can be spread over more bins, we consider the target ranging correctly performed if the error is contained within 30 cm (i.e. at most two bins far from the one containing the target TOA).<sup>11</sup>

Fig. 8 shows the performance when the intended useful target has a RCS  $\zeta_u$  uniformly distributed between 0 and  $\zeta_u^{\max} = (\zeta_i^{\max}/100) \text{ m}^2$  (i.e.  $\rho = 100$ ) and  $\zeta_u^{\max} = (\zeta_i^{\max}/500) \text{ m}^2$  (i.e.  $\rho = 500$ ), for  $N_{\text{array}} = 15 \times 15$  and  $N_{\text{array}} = 20 \times 20$ . The receiver operating characteristics (ROCs) of CDR have been obtained by imposing  $P_{\text{SC}}^* = 10^{-3}$ , and by setting the RCS  $\zeta$ ,

<sup>10</sup>Note that here the FRR is related to the simulated PFR which refers to situations 3 and 4 of Fig. 6. On the contrary, the CDR refers to situations 2, 3 and 4 of the same Figure.

<sup>11</sup>Finer procedures can be then adopted to reduce the ranging error.

for the NCP, from 0.1 to  $1 \text{ m}^2$  with step 0.1.

From the obtained results it is evidenced that if 400 elements are adopted, the requirement in terms of phase quantization bits can be relaxed in favor of good performance for each scanning direction. On the contrary, for  $N_{\text{array}} = 15 \times 15$ , at least 2 phase quantization bits are necessary in order to guarantee robust performance to interferers. In fact, when 1 phase quantization bit is adopted, the achieved FRR drastically increases with  $\theta_b = 20^\circ$ . Thus, there is a trade-off between the number of elements, which guarantees also better detection and localization performance, the number of quantization bits and the overall system complexity.

2) *Results with Multiple Interferers:* In order to test the system robustness to multiple interferers, we consider 10 interferers with RCS uniformly distributed within 0 and  $1 \text{ m}^2$ , with one always in the main side-lobe direction and the others uniformly distributed between the entire pattern apart from the main direction. The ROCs have been obtained by imposing  $P_{\text{SC}}^* = 10^{-3}$ , and by setting the RCS  $\zeta$ , for the NCP, from 0.1 to  $2 \text{ m}^2$  with step 0.1. In such scenario, we fixed  $\rho = 100$ , which is a reasonable value found from measured data.

From Fig. 9 it is possible to observe that with 1 phase quantization bit, a  $\text{CDR} = 80\%$  with  $\text{FRR} = 4\%$  (marked with the ellipse in the figure) is still attainable for the steering direction  $\theta_b = 60^\circ$ . For both  $15 \times 15$  and  $20 \times 20$  elements, 2 phase bits guarantee performance robust to the environment.

The obtained simulation results suggest that with a proper joint threshold-array design, it is possible to achieve the attainable desired performance even in harsh cluttered environments. Furthermore, despite the large number of antenna elements employed, the complexity of the architecture can be kept low thanks to the adoption of a low number of quantization bits, as happened when  $20 \times 20$  arrays with 1 bit of phase quantization were used. In the following, such architecture is tested in order to provide the preliminary feasibility of the proposed joint threshold-array design even in real indoor environments.

### B. Measurement Results

In order to show the feasibility of the proposed detection scheme with real data, we conducted a measurement campaign at CEA LETI office environment, Grenoble. As an input of the measurement analysis, we consider the array configuration  $20 \times 20$  with 1 bit of phase quantization, which has been shown as a good compromise between complexity and achievable performance through the simulation analysis.

Thus, to achieve our goal, we conducted two measurements campaigns: first, we characterized the RCS of a metallic plate in order to set the threshold and the level of interference for simulated data, and successively we mechanically steered a massive array in different positions within a corridor, to see if walls are correctly detected and localized as it should happen in personal radars applications, where users walk in indoor environments, such as corridors. In particular, the measurement set-up consists of a 4-ports vector network analyzer operating in the frequency range 10 MHz-24 GHz, connected to 2 mmW converters operating in the frequency range 50 GHz-75 GHz and to 2 linearly polarized TAs, described in the following. A

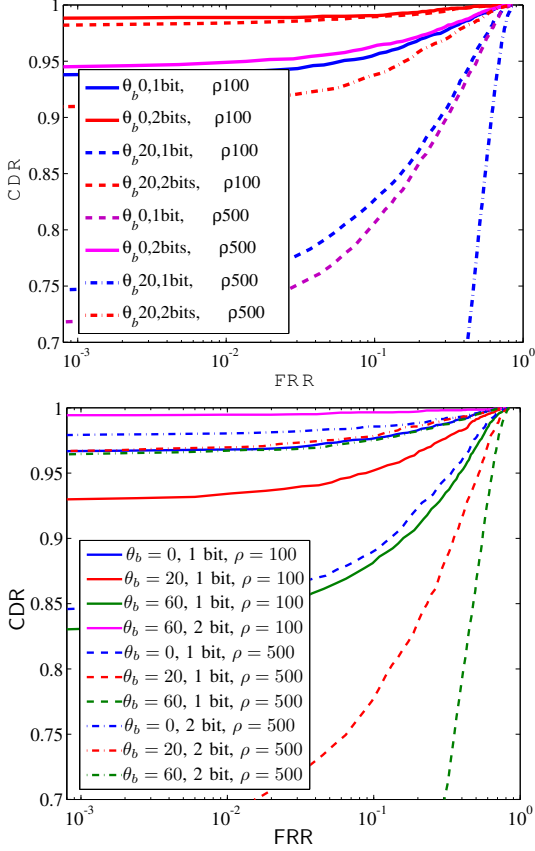


Fig. 8. Correct detection rate vs false ranging rate with  $15 \times 15$  arrays (top) and  $20 \times 20$  array (bottom) in the presence of 1 interferer.

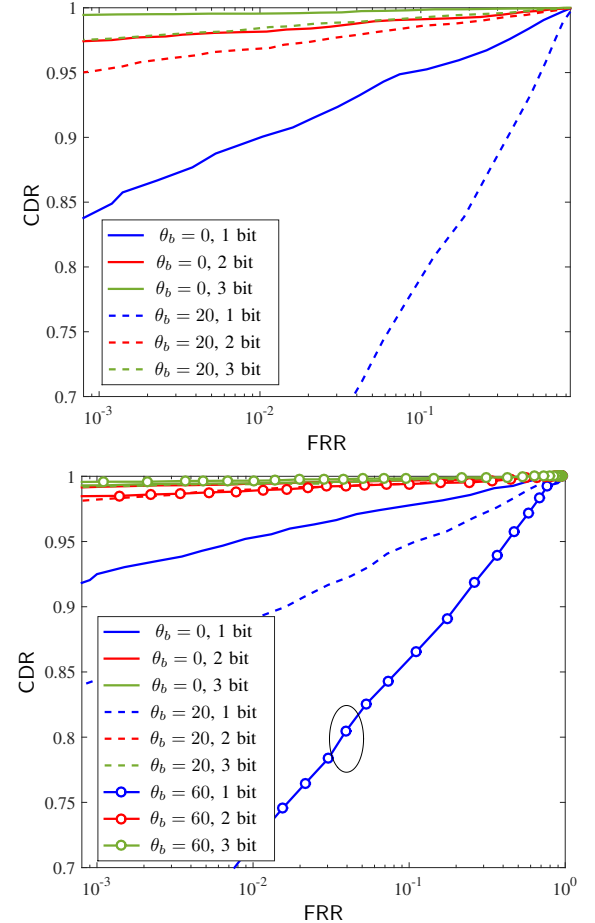


Fig. 9. Correct detection rate vs false ranging rate with  $15 \times 15$  arrays (top) and  $20 \times 20$  array (bottom) in the presence of 10 interferers and  $\rho = 100$ .

bistatic configuration has been considered with the TAs spaced apart of 0.16 m in order to mitigate the antenna coupling and to separate the transmitting and receiving channels. A detailed description of the measurement campaign is reported in [45]. For our specific scenario, we consider a point in the environment with 15 mechanically steered directions allowed by the adopted *X-Y-Azimuth* positioner, in the frequency range between 59.5 – 60.5 GHz with a step of 5 MHz. For the considered measurement position, the *X-Y-Azimuth* positioner permits to rotate the radar in the semi-plane from  $-45^\circ$  to  $45^\circ$  with a step of  $5^\circ$  (in accordance to the HPBW of the TA used) in order to emulate the beamforming operation in a realistic scenario. This mechanical steering is imposed by the fact that the considered TA prototype is non-reconfigurable.

a) *Measured Massive Arrays Characteristics:* We exploited the TAs, described in [18], as  $20 \times 20$  massive arrays with 1 bit of phase quantization. They consist of a focal source, that is a 10.2 dBi linearly-polarized pyramidal horn antenna working in the V-band, illuminating a planar array with  $20 \times 20$  unit-cells, each with size  $2.5 \times 2.5$  mm $^2$ . Each unit-cell is composed of two patch antennas rotated in order to create a precise phase value to steer the beam. For the considered case, they are not reconfigurable but with a fixed beam in the direction  $\theta_b = 0^\circ$ . The 1-bit of phase compensation corresponds to two possible phase values ( $0^\circ$  and  $180^\circ$ ) [18], with a maximum gain of 23.3 dBi.

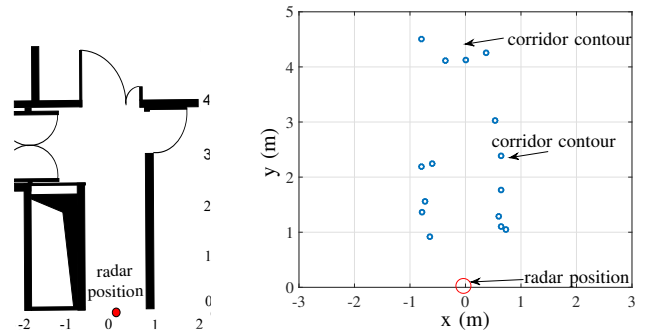


Fig. 10. Measurement results obtained in the corridor environment. In the results, the reference point has been set to the radar position.

As previously mentioned, such array characteristics are matching with the need to have extremely high directive antennas in order to scan the environment in localization and mapping applications as the personal radar one.

b) *Results:* According to the output from simulations and the array choice, we now only need to estimate a proper value of  $\zeta_i$  for the threshold design. Thus, from the measurement of a metallic plate with size  $0.7 \times 0.7$  m $^2$  at a distance of 1.1 m from the array, we found a value around 1 m $^2$ .

In Fig. 10 we report the environment reconstruction from the considered radar position by using the 1-bit massive array and

receiver section previously described. The proposed algorithm permits to achieve a localization error of at most few bins which corresponds to the TOA resolution determined by the size of the time bins ( $T_{ED} = 1$  ns). As a consequence, a first reconstruction of the environment including doors, walls and metallic objects detection can be achieved using the proposed antennas and receiver scheme.

The same measurements have been also post-processed by adopting a classical CFAR approach accounting for a laser-like antenna in the threshold design, with the impossibility to reconstruct the map because of the side-lobes and antennas coupling residuals.

## VI. CONCLUSIONS

In this paper we analysed the impact of massive arrays side-lobes into detection performance for mapping/SLAM and personal radars applications. In particular, in order to keep both the antenna array complexity and the cost low, a discrete set of phase shifts is often adopted for beamforming at the expense of an increased side-lobe level. In these situations, the design of a threshold accounting only for the receiver noise is not sufficient to guarantee the correct functioning of the system in terms of detection performance. In fact, as demonstrated by simulation results, the presence of side-lobes could drastically increase the false alarm probability even when there is no target in the steering direction. This effect poses several attentions in the massive array design according to its maximum acceptable SLL. Successively, we have shown the joint conception of a massive array mask and of a thresholding strategy robust to the presence of interferers in the side-lobes direction. The proposed scheme has been validated through simulated and measured data with real massive arrays with  $20 \times 20$  elements. Results underline that the proposed scheme is robust to the array impairments even when the number of phase-bits is low in favor of a reduced system complexity.

## ACKNOWLEDGMENT

This research was supported in part by the IF-EF Marie-Curie project MAPS (Grant 659067) and by the European H2020 project XCycle (Grant 635975). Authors would like to thank Nicoló Decarli and Andrea Mariani for fruitful discussions.

## REFERENCES

- [1] W. Hong *et al.*, "Study and prototyping of practically large-scale mmwave antenna systems for 5G cellular devices," *IEEE Commun. Mag.*, vol. 52, no. 9, pp. 63–69, 2014.
- [2] W. Roh *et al.*, "Millimeter-wave beamforming as an enabling technology for 5G cellular communications: theoretical feasibility and prototype results," *IEEE Commun. Mag.*, vol. 52, no. 2, pp. 106–113, 2014.
- [3] M. W. M. G. Dissanayake *et al.*, "A solution to the simultaneous localization and map building (SLAM) problem," *IEEE Trans. Robot. Autom.*, vol. 17, no. 3, pp. 229–241, Jun 2001.
- [4] E. Jose *et al.*, "Predicting Millimeter Wave Radar Spectra for Autonomous Navigation," *IEEE Sensors J.*, vol. 10, no. 5, pp. 960–971, May 2010.
- [5] F. Guidi, A. Guerra, and D. Dardari, "Personal mobile radars with millimeter-wave massive arrays for indoor mapping," *IEEE Trans. Mobile Comp.*, vol. 15, no. 6, pp. 1471–1484, Jun. 2016.
- [6] K. Witrisal *et al.*, "High-accuracy localization for assisted living," *IEEE Signal Processing Mag.*, 2016.
- [7] X. Huang and Y. Guo, "Frequency-domain AoA estimation and beam-forming with wideband hybrid arrays," *IEEE Trans. Wireless Commun.*, vol. 10, no. 8, pp. 2543–2553, August 2011.
- [8] J. Zhang *et al.*, "Massive hybrid antenna array for millimeter-wave cellular communications," *IEEE Wireless Commun.*, vol. 22, no. 1, pp. 79–87, Feb. 2015.
- [9] A. Clemente *et al.*, "Wideband 400-Element Electronically Reconfigurable Transmitarray in X Band," *IEEE Trans. Antennas Propag.*, vol. 61, no. 10, pp. 5017–5027, Oct 2013.
- [10] A. Guerra *et al.*, "Application of transmitarray antennas for indoor mapping at millimeter-waves," in *Proc. IEEE European Conf. on Networks and Commun. (EUCNC)*, 2015.
- [11] D. Dardari *et al.*, "Ranging with ultrawide bandwidth signals in multi-path environments," *Proc. IEEE*, vol. 97, no. 2, pp. 404–426, Feb 2009.
- [12] Y. Shen and M. Win, "Fundamental limits of wideband localization; part I: A general framework," *IEEE Trans. Inf. Theory*, vol. 56, no. 10, pp. 4956–4980, oct. 2010.
- [13] A. Guerra, F. Guidi, and D. Dardari, "Position and orientation error bound for wideband massive antenna arrays," in *Proc. IEEE Int. Conf. on Commun. (ICC), ANLN Workshop*, June 2015, pp. 853–858.
- [14] D. Jourdan, D. Dardari, and M. Win, "Position error bound for UWB localization in dense cluttered environments," *IEEE Trans. Aerosp. Electron. Syst.*, vol. 44, no. 2, pp. 613–628, April 2008.
- [15] A. Clemente *et al.*, "1-Bit Reconfigurable Unit Cell Based on PIN Diodes for Transmit-Array Applications in X-Band," *IEEE Trans. Antennas Propag.*, vol. 60, no. 5, pp. 2260–2269, May 2012.
- [16] L. Rondinelli, "Effects of random errors on the performance of antenna arrays of many elements," in *IRE Int. Convention Record*, vol. 7, March 1959, pp. 174–189.
- [17] J. Ruze, "Antenna tolerance theory - a review," *Proc. IEEE*, vol. 54, no. 4, pp. 633–640, April 1966.
- [18] H. Kaouach *et al.*, "Wideband low-loss linear and circular polarization transmit-arrays in V-band," *IEEE Trans. Antennas Propag.*, vol. 59, no. 7, pp. 2513–2523, July 2011.
- [19] J. Krieger, C.-P. Yeang, and G. Wornell, "Dense delta-sigma phased arrays," *IEEE Trans. Antennas Propag.*, vol. 61, no. 4, pp. 1825–1837, 2013.
- [20] F. Guidi *et al.*, "Energy detection performance with massive arrays for personal radars applications," in *Proc. 11th EAI Int. Conf. on Cognitive Radio Oriented Wireless Networks (CROWNCOM)*, May 2016.
- [21] R. L. Haupt, "Phase-only adaptive nulling with a genetic algorithm," *IEEE Trans. Antennas Propag.*, vol. 45, no. 6, pp. 1009–1015, Jun 1997.
- [22] J.-H. Lee and Y.-H. Lee, "Two-dimensional adaptive array beamforming with multiple beam constraints using a generalized sidelobe canceller," *IEEE Trans. Signal Processing*, vol. 53, no. 9, pp. 3517–3529, Sept 2005.
- [23] D. J. Rabideau, "Multidimensional sidelobe target editing with applications to terrain scattered jamming cancellation," in *Proc. Ninth IEEE SP Workshop on Statistical Signal and Array Processing*, Sep 1998, pp. 252–255.
- [24] E. Kelly, "An adaptive detection algorithm," *IEEE Trans. Aerosp. Electron. Syst.*, vol. AES-22, no. 2, pp. 115–127, March 1986.
- [25] U. Nickel, "Detection with adaptive arrays with irregular digital subarrays," in *Proc. IEEE Radar Conf.*, April 2007, pp. 635–640.
- [26] C. Richmond, "Performance of the adaptive sidelobe blanker detection algorithm in homogeneous environments," *IEEE Trans. Signal Process.*, vol. 48, no. 5, pp. 1235–1247, May 2000.
- [27] K. Sangston, F. Gini, and M. Greco, "Coherent radar target detection in heavy-tailed compound-Gaussian clutter," *IEEE Trans. Aerosp. Electron. Syst.*, vol. 48, no. 1, pp. 64–77, Jan 2012.
- [28] J. Tsao and B. Steinberg, "Reduction of sidelobe and speckle artifacts in microwave imaging: the CLEAN technique," *IEEE Trans. Antennas Propag.*, vol. 36, no. 4, pp. 543–556, Apr 1988.
- [29] H. Deng, "Effective CLEAN algorithms for performance-enhanced detection of binary coding radar signals," *IEEE Trans. Signal Process.*, vol. 52, no. 1, pp. 72–78, Jan 2004.
- [30] A. Martinez *et al.*, "Energy detection using very large antenna array receivers," in *Proc. IEEE 48th Asilomar Conf. Signals, Syst. and Comput.*, Nov 2014, pp. 1034–1038.
- [31] W. Jiang and A. M. Haimovich, "Cramer-rao bound and approximate maximum likelihood estimation for non-coherent direction of arrival problem," in *Annual Conf. on Inf. Science and Syst. (CISS)*, March 2016, pp. 506–510.

- [32] S.-H. Wu *et al.*, "Robust hybrid beamforming with phased antenna arrays for downlink SDMA in indoor 60 Ghz channels," *IEEE Trans. Wireless Commun.*, vol. 12, no. 9, pp. 4542–4557, September 2013.
- [33] L. Stoica, A. Rabbachin, and I. Oppermann, "A low-complexity non-coherent IR-UWB transceiver architecture with TOA estimation," *IEEE Trans. Microw. Theory Tech.*, vol. 54, no. 4, pp. 1637–1646, Jun. 2006.
- [34] K. Witrisal *et al.*, "Noncoherent ultra-wideband systems," *IEEE Signal Process. Mag.*, vol. 26, no. 4, pp. 48–66, Jul. 2009.
- [35] H. Urkowitz, "Energy detection of unknown deterministic signals," *Proc. IEEE*, vol. 55, no. 4, pp. 523 – 531, april 1967.
- [36] D. Slepian and E. Sonnenblick, "Eigenvalues associated with prolate spheroidal wave functions of zero order," *Bell Sys. Tech. Journal*, vol. 44, 1965.
- [37] M. Abramowitz and I. A. Stegun, *Handbook of Mathematical Functions with Formulas, Graphs, and Mathematical Tables*. Washington, D.C.: United States Department of Commerce, 1970.
- [38] A. Mariani, A. Giorgetti, and M. Chiani, "Effects of noise power estimation on energy detection for cognitive radio applications," *IEEE Trans. Commun.*, vol. 59, no. 12, pp. 3410–3420, Dec. 2011.
- [39] L. Di Palma *et al.*, "1-bit reconfigurable unit-cell for ka-band transmimarrays," *IEEE Antennas and Wireless Propag. Lett.*, vol. PP, no. 99, pp. 1–1, 2015.
- [40] P. Baltus, P. Smulders, and Y. Yu, *Systems and Architectures for Very High Frequency Radio Links*. Springer Netherlands, 2008.
- [41] B. Wu *et al.*, "On the selection of the number of bits to control a dynamic digital MEMS reflectarray," *IEEE Antennas and Wireless Propag. Lett.*, vol. 7, pp. 183–186, 2008.
- [42] F. Guidi *et al.*, "Detection of multiple tags based on impulsive backscattered signals," *IEEE Trans. Commun.*, vol. 62, no. 11, pp. 3918–3930, Nov 2014.
- [43] M. Chiani, "Integral representation and bounds for marcum Q-function," *IEEE Electronics Lett.*, vol. 35, no. 6, pp. 445–446, Mar. 1999.
- [44] S. Y. Chun and A. Shapiro, "Normal versus noncentral chi-square asymptotics of misspecified models," *Multivariate Behavioral Research*, vol. 44, no. 6, pp. 803–827, 2009.
- [45] A. Guerra *et al.*, "Millimeter-wave backscattering measurements with transmimarrays for personal radar applications," in *Proc. IEEE Global Conf. on Commun. (GLOBECOM), LION Workshop*, 2015.



**Anna Guerra** (M'16) received the B.S. degree and the M.S. from the University of Bologna in electronics and telecommunications engineering in 2009 and 2011, respectively. In 2012, she was a research assistant in a collaboration project between the Consorzio Nazionale Interuniversitario per le Telecomunicazioni (CNIT) and French Atomic Energy Commission (CEA-LETI), Grenoble, France. From mid-2014 to mid-2015, she was a visiting student at CEA-LETI, Grenoble, France. In 2016, she received the PhD degree in electronics, telecommunications, and information technologies at the University of Bologna, Italy. She received the best student paper award at the 2014 IEEE International Conference on Ultra-Wideband in Paris, France. Her research interest includes radio localization and mapping, array signal processing, UWB, and millimeter-wave technology.



**Davide Dardari** (M'95-SM'07) received the Laurea degree in electronic engineering (summa cum laude) and the PhD degree in electronic engineering and computer science from the University of Bologna, Italy, in 1993 and 1998, respectively. He is an Associate Professor at the University of Bologna at Cesena, Italy, where he participates with WiLAB (Wireless Communications Laboratory). Since 2005, he has been a Research Affiliate at Massachusetts Institute of Technology (MIT), Cambridge, USA. He is also Research Affiliate at IEIIT/CNR (National Research Council) and CNIT (Consorzio Nazionale Interuniversitario per le Telecomunicazioni). He published more than 150 technical papers and played several important roles in various National and European Projects. His interests are on wireless communications, localization techniques, and distributed signal processing. He received the IEEE Aerospace and Electronic Systems Society's M. Barry Carlton Award (2011) and the IEEE Communications Society Fred W. Ellersick Prize (2012). Prof. Dardari is Senior Member of the IEEE where he was the Chair for the Radio Communications Committee of the IEEE Communication Society. He was co-General Chair of the 2011 IEEE International Conference on Ultra-Wideband and co-organizer of the IEEE International Workshop on Advances in Network Localization and Navigation (ANLN) - ICC 2013-2016 editions. He was also co-Chair of the Wireless Communications Symposium of the 2007/2017 IEEE International Conference on Communications, and co-Chair of the 2006 IEEE International Conference on Ultra-Wideband. He served as Lead Editor for the EURASIP Journal on Advances in Signal Processing (Special Issue on Cooperative Localization in Wireless Ad Hoc and Sensor Networks), Guest Editor for Proceedings of IEEE (Special Issue on UWB Technology & Emerging Applications), for the Physical Communication Journal (ELSEVIER) (Special Issue on Advances in UWB Wireless Communications) and for IEEE Trans. on Vehicular Technology (Special Session on indoor localization, tracking, and mapping with heterogeneous technologies). He served as an Editor for IEEE TRANSACTIONS ON WIRELESS COMMUNICATIONS from 2006 to 2012.



**Francesco Guidi** (S'09 - M'14) received the B.S. degree and the M.S. degree (both summa cum laude) from the University of Bologna in biomedical (2006) and in electronics and telecommunications (2009) engineering, respectively. In 2013 he received the PhD degree both from Ecole Polytechnique Paris-Tech, France (Computer Science Specialty) and from University of Bologna, Italy, in electronics, telecommunications and information technologies.

He is currently a Marie Curie Fellow at CEA-LETI, Grenoble, France. From mid-2013 to mid-2015 he was a postdoctoral researcher at University of Bologna. His research interests include RFID and radar technologies, joint antenna and channel characterization, signal processing, UWB and mm-waves technologies. He was the recipient of the best student paper award at the 2014 IEEE International Conference on Ultra-Wideband. Dr. Guidi serves as reviewer for numerous IEEE Journals and Conferences and was a member of the local organization committee for the 2011 IEEE International Conference on Ultra-Wideband.



**Antonio Clemente** (S'11 - A'13 - M'14) received the B.S. and M.S. degree in telecommunication engineering and remote sensing systems from the University of Siena, Italy, in 2006 and 2009, and the Ph.D. degree in signal processing and telecommunications from the University of Rennes 1, France, in 2012. From October 2008 to May 2009 he realized his master thesis project at Technical University of Denmark (DTU), Lyngby, Denmark, where he worked on spherical near-field antenna measurements. His Ph.D. has been realized at CEA-LETI, Grenoble, France. In 2012, he joined the R&D laboratory of Satimo Industries, Villebon-sur-Yvette, France. Since 2013, he is a Research Engineer at CEA-LETI, Grenoble, France. His current research interests include fixed-beam and electronically reconfigurable transmitarray antennas at microwave and millimeter-wave frequencies, antenna arrays, miniature integrated antennas, antenna fundamental limitations, near-field and far-field antenna measurements. He serves as reviewer for numerous IEEE and IET journals in the field of Microwave, Antennas and Propagation. Dr. Clemente received the Young Scientist Awards (First Prize) during the 15th International Symposium of Antenna Technology and Applied Electromagnetics 2012 (ANTEM 2012) and he is co-recipient of the Best Paper Awards at JNM2015 (19emes Journées Nationales Microondes).



**Raffaele D'Errico** received the Laurea (summa cum laude) degree in telecommunications engineering from the University of Bologna, Bologna, Italy, in 2005, and the Ph.D. degree from the University of Paris-Sud, Orsay, France, and the University of Bologna, in 2008. He has been a Research Engineer and Project Manager with CEA-LETI, Grenoble, France, since 2008. He was involved in several FP7 and H2020. He participated to COST 2100 and IC1004 activities, as the Chairman of the Working Group Body Environments, and currently to the IRACON action. His current research interests include channel modeling for mobile communication, wireless sensor networks and body area networks, small antenna design, ultrawideband (UWB) and UHF RFID, UWB localization, millimeter-wave channel, and OTA tests. Dr. D'Errico authored or coauthored three best paper awards at the IEEE PIMRC 2009, the IFIP NTMS 2011, and the LAPC 2012 Best Student Paper.